IRA-International Journal of Applied Sciences
ISSN 2455-4499; Vol.21, Issue 02 (Q2. 2026)
Pg. no. 29-54.
IRA Academico Research

Theoretical and Experimental Study of The Performance of The Flat-Plate Thermosiphon Collector of A Solar Water Heater Using Locally Available Materials

André Luc Batiana[1,2#], Salmwendé Eloi Tiendrebeogo[2,3], Emmanuel Sidwaya Sawadogo[1,2], Guy Christian Tubreoumya[1,2], Désiré Zerbo[1,2], Alfa Oumar Dissa[1,2]
[1]University Joseph KI-ZERBO, Ouagadougou, Burkina Faso (UJKZ).
[2]Laboratory of Environmental Physics and Chemistry (LPCE) Université Joseph Ki Zerbo Ouagadougou, Burkina Faso.
[3]Ecole Normale Supérieur Ouagadougou, Burkina Faso.
[4]University Lédéa Bernard OUEDRAOGO Ouahigouya, Burkina Faso.

[#]corresponding author
Type of Work: Peer Reviewed.
DOI: https://dx.doi.org/10.21013/jas.v21.n2.p1

Review history: Submitted: February 25, 2026; Revised: April 18, 2026; Accepted: May 2, 2026.

How to cite this paper:
Batiana, A. L, Tiendrebeogo, S. E., Sawadogo, E. S., Tubreoumya, G. C., Zerbo, D. & Dissa, A. O. (2026). Theoretical and Experimental Study of The Performance of The Flat-Plate Thermosiphon Collector of A Solar Water Heater Using Locally Available Materials. *IRA-International Journal of Applied Sciences* (ISSN 2455-4499), 21(2), 29-54. https://dx.doi.org/10.21013/jas.v21.n2.p1

ABSTRACT

Our work focuses on a numerical and experimental study of a flat plate solar collector designed and tested at the Ecole Normale Supérieure (ENS) in Burkina Faso at the Ouagadougou annex site. This device converts solar radiation into thermal energy. It was designed using locally available materials by a local designer. The objective of our work is to study temperature changes, efficiency, and the impact of solar radiation on the system during a less sunny period (rainy weather) that is conducive to the use of domestic hot water in order to evaluate its performance and provide solutions to optimize the device's efficiency and performance. The numerical results show that the average water temperature is 33°C compared to 49°C for the experimental results, with a theoretical efficiency of around 70%. Our results show that this device can heat water during the day despite unfavorable meteorological conditions.

Keywords: Thermal energy, water heater, solar collector, optimization.

1. Introduction

Solar energy is currently one of the most promising sources for meeting global energy needs. This energy has the advantage of being clean and renewable, with 169,440 TWh per year of sunshine (BOUALAMALLAH et al., 2021). Solar water heating systems can be used in all climates. However, their performance varies depending on the amount of solar energy available in the region and, above all, the temperature of the water entering the system: the colder the incoming water, the higher the efficiency of the solar water heater(Sunday S. Nunayon et al., 2022), and BURKINA FASO is ranked as one of the countries with the most abundant solar energy. The development and use of this energy could reduce the use of conventional sources, which are polluting and harmful to the planet, according to the Energy Sector Regulatory Authority(*ARSE - Burkina Faso*, n.d.) and (KY, 2024). When determining the performance of a solar water heater installed at a given site, the parameters used for the calculation are generally averaged. This is true for determining long-term performance, but does not reflect actual performance behavior on a daily basis due to fluctuations in weather parameters(S.A. Hakem et al., 2008). In addition, the thermosiphon solar system, or natural circulation solar water heater, is the most interesting, simplest, and most popular technological device used for solar energy exploitation. The overall objective of this work is to numerically evaluate the external and internal parameters influencing the performance of the solar collector; to compare the numerical and empirical results under unfavorable weather conditions; and to study possible improvements to optimize the collector, giving priority to locally available materials. Specifically, we studied:

- The evolution of global radiation;
- The evolution of the average temperature of the heat transfer fluid
- The evolution of the temperatures of the collector components and the useful power
- The instantaneous numerical and experimental efficiency of the flat-plate solar collector.
- The mass flow rate

2. Materials and Methods

The solar prototype under study was designed and built in Burkina Faso by a local company called Atelier Nikiema&frère. It was installed on the premises of the teacher training college in 2020. The water heater is a separate-component type consisting of a solar collector and a storage tank.

2.1 Description of the flat plate solar collector (figure 1)

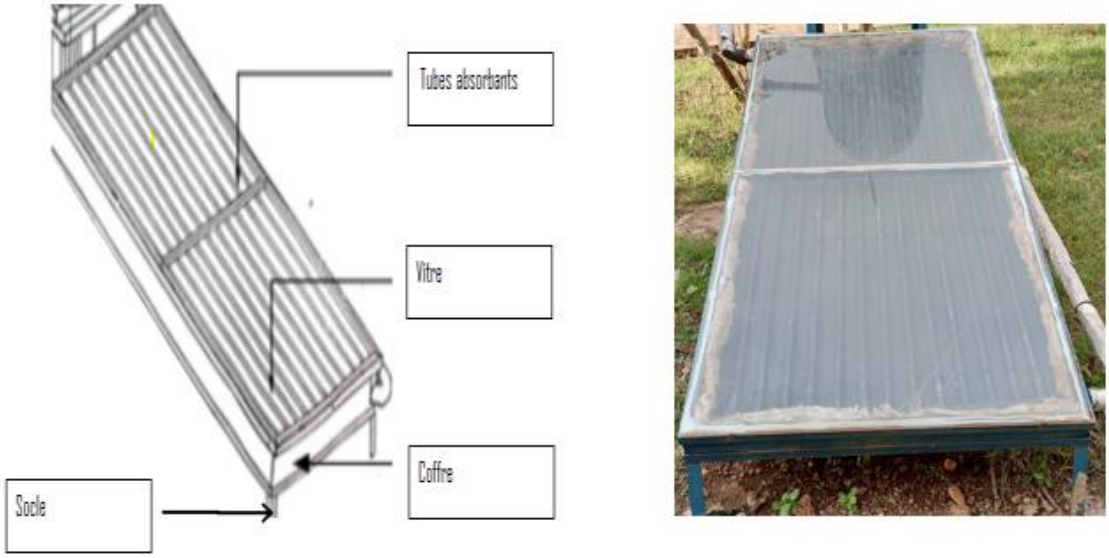

Figure 1 : Components of the thermosiphon solar collector

2.2 Experimental study

2.2.1 Site

The water heater is installed in Burkina Faso at the Institute of Science in the city of Ouagadougou (latitude 12°21'45“ North, longitude 1°29'21.8” West). The water heater is fixed to the ground next to a two-story building that serves as student accommodation.

2.2.2 Equipements de mesures

Water is stored in a cylindrical tank placed vertically above the solar collector on a base. Three key criteria were used to select and use the materials: availability, acceptable cost, and thermal properties.

- Thermocouple

A thermocouple is a sensor used to measure temperature. Our thermocouple (photo 2) is type K, with a chrome metal positive (+) pole and an aluminum metal negative (-) pole, with a measurement error of plus or minus 1.5°C. **(figure 2)**

- Data logger

The thermocouples are connected to a data recording unit called a data logger. The data logger used is a Keithley type with an uncertainty of 1%. To power the data logger, we used energy produced by SONABEL **(figure 2)**

- The solarimeter

The solarimeter is the device used to measure global radiation. It is placed on the surface of our sensor with the same inclinations. The error made by the device during a given measurement is estimated at 5%. **(figure 2)**

Solarimeter Type K thermocouple Keithley data logger

Figure 2 : Experimental data measurement equipment

2.2.3 Experimental protocol

This work, we focused primarily on global radiation and component temperatures at the sensor level. These data will enable us to study the actual performance of this system. Temperature measurements are taken using type K thermocouples attached to the surface of the system where the temperature is to be measured. The thermocouples are held in place using aluminum adhesive tape. The solar meter, used to measure solar radiation, is placed on the system's glass panel at the same angle as the panel. Finally, all of the thermocouples and the solar meter are connected to a data logger, which automatically records the data on a USB drive for subsequent processing on a computer.

2.3 Instantaneous efficiency estimate Experimental

Efficiency of ηcap sensors in (%) :(ARMAND NOËL NGUECHE CHEDOP et al., 2018)

$\eta_{cap} = \beta - a_1 \frac{[T_m - T_a]}{G} - a_2 \frac{[T_m - T_a]^2}{G}$ (John A. Duffie (Deceased) & William A. Beckman, 2013) **(1)**

$\beta = \alpha \times \tau$ **(2)**

$T_m = (T_e - T_s) \div 2$ (3)

The efficiency ($\boldsymbol{\eta cap}$) depends on the amount of sunlight and the temperature difference between the ambient environment and the absorber. It is zero when the heat transfer fluid is shut off.

- Power received by the absorber P absorber in (W/m^2)

$P_{absorbeur} = \beta \times I_s$ (4)

- Useful power of the absorber (P_useful) per unit of collector surface area (W/m^2): is the power transferred to the water.

$P_{utile} = P_{absorbeur} - Heat\ loss$ (5)

$$P_{utile} = \beta \times I_s - \kappa \times [T_m - T_a] \quad (7)$$

$$P_{utile} = \eta_{cap} \times I_s \quad (8)$$

• Useful power (P_{U_t}) total solar collector in (W)

$$P_{U_t} = sensor\ aperture\ area \times P_{utile}$$

$$P_{U_t} = \eta_{cap} \times I_s \times S \quad \textbf{(9)}$$

3. Theoretical Study

3.1 Simplifying assumptions

- ✓ The sky radiates at the TC temperature calculated using an empirical formula;
- ✓ Diffuse solar radiation is isotropic;
- ✓ The ground temperature is taken to be equal to the ambient temperature;
- ✓ The flow regime is transient;
- ✓ The physical properties (mass, density, thickness) of the materials are assumed to be constant and independent of temperature;
- ✓ The surfaces of the glass, the absorbing plate, and the insulation are isothermal;
- ✓ The surfaces where radiative exchanges occur are considered to be diffuse gray.
- ✓ The inner walls of the tubes are perfectly smooth so that losses due to roughness can be neglected.
- ✓ The side walls and rear face of the collector are insulated.
- ✓ The glass is opaque to infrared radiation emitted by the absorber.
- ✓ Exchanges between the ground and the device are negligible.

3.2 Physical model and equivalent electrical diagram (M. BOURAGBI Lakhdarn, 2024)

The figure 3 shows physical model and equivalent electrical diagram

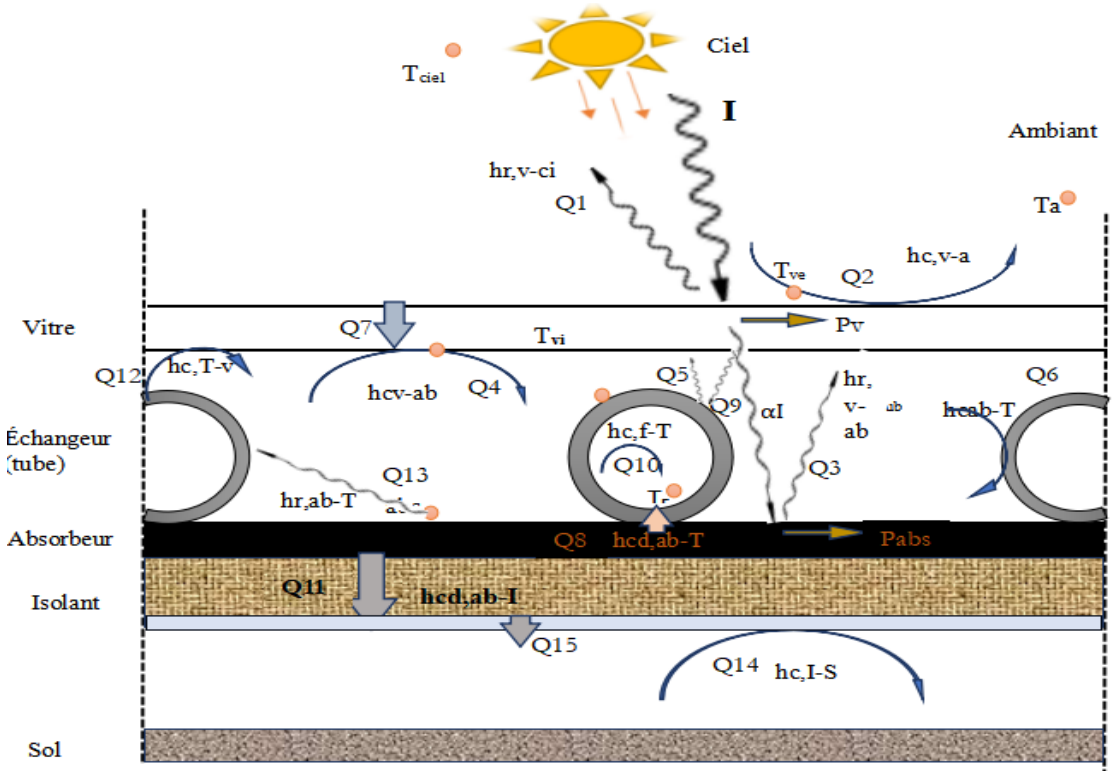

Figure 3 : Physical model of the solar collector

The electrical analogy related to the different thermal resistances during heat exchanges carried out on the different elements of the sensor is illustrated in **Figure 4**.(Michel Daguenet, 1985)

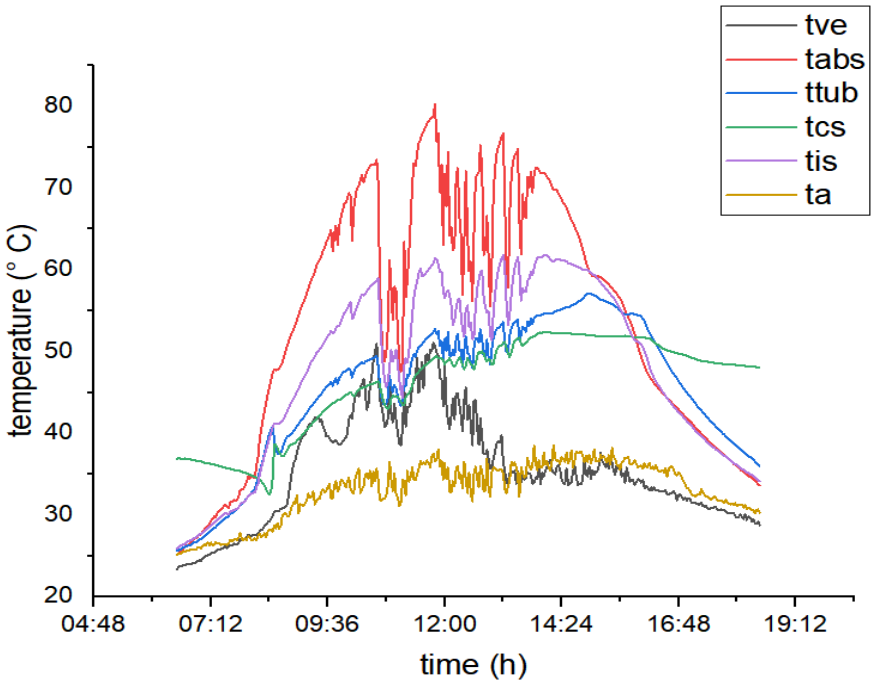

Figure 4 : Electrical diagram of the solar sensor

3.3 Energy and thermal balance (*Article_KABORE_Elixir (2).Pdf*, n.d.)

To establish the heat balance that reflects the behavior of our sensor, the nodal method was applied.

Energy balance of the outer surface of the glass pane

$$\frac{1}{2}M_v C_{pv}\frac{dT_{ve}}{dt} = hr_{ci}S_v(T_{ci}-T_{ve}) + hc_v S_v(T_a - T_{ve}) + hcd_v S_v(T_{vi}-T_{ve}) + \alpha_v I_G S_v \quad \textbf{(10)}$$

Energy balance of the inner surface of the glass pane

$$\frac{1}{2}M_v C_{pv}\frac{dT_{vi}}{dt} = hr_{v-t}S_v(T_t - T_{vi}) + hc_{v-t}S_v(T_t - T_{vi}) + hc_{v-ab}S_v(T_{ab}-T_{vi}) + hr_{v-t}S_v(T_{ab}-T_{vi}) + hcd_v S_v(T_{vi}-T_{ve}) \quad \textbf{(11)}$$

Energy balance of the tube

$$M_t C_{pt}\frac{dT_t}{dt} = hr_{t-v}S_t(T_{vi}-T_t) + hr_{ab-t}S_t(T_{ab}-T_t) + hc_{t-v}S_t(T_{vi}-T_t) + hcd_{ab}S_t(T_{ab}-T_t) + hc_{t-f}A_t(T_f - T_t) + \alpha_t\tau_v I_G S_t \quad \textbf{(12)}$$

Energy balance of the heat transfer fluid

$$\rho_e C_{pe}\frac{D_h}{4}\frac{dT_f}{dt} + \rho_e C_{pe}\frac{\dot{m}D_h}{4n}\frac{dT_f}{dx} = hc_{t-f}A_t(T_f - T_t) \quad \textbf{(13)}$$

Energy balance of the absorber plate

$$M_{ab}C_{pab}\frac{dT_{ab}}{dt} = hr_{ab-v}S_{ab}(T_{vi}-T_{ab}) + hr_{ab-t}S_{ab}(T_t - T_{ab}) + hc_{ab-v}S_{ab}(T_{vi}-T_{ab}) + hcd_{ab}S_t(T_t - T_{ab}) + hcd_{is}A_{ab}(T_{is}-T_{ab}) + \alpha_{ab}\tau_v I_G S_{ab} \quad \textbf{(14)}$$

Energy balance of the internal insulation

$$M_{is}C_{pis}\frac{dT_{is}}{dt} = hcd_{is-b}S_{is}(T_b - T_{is}) + hcd_{ab}S_{ab}(T_{ab}-T_{is}) \quad \textbf{(15)}$$

Energy balance of the external insulation

$$M_{is}C_{pis}\frac{dT_{is}}{dt} = hc_{b-a}S_b(T_a - T_b) + hcd_b S_b(T_{is}-T_b) \quad \textbf{(16)}$$

This gives us a system of equations with six unknowns:

$\boldsymbol{T_{ve}, T_{vi}, T_t, T_f, T_{ab}, T_{is}, T_b}$

- heat transfer coefficients

convective heat transfer coefficient of the air confined between the inner surface of the glass and the absorbing plate

$$h_{c,vi} = h_{c,ab} = h_{c,tub} = \frac{\lambda_{air}Nu}{e_1} \quad \textbf{(17)}$$

Pour l'air

$$Nu = \left[0.06 - 0.017\left(\frac{\beta}{90}\right)\right]G_r^{1/3} \quad \textbf{(18)}$$

$$G_r = \frac{g.\Delta T.e_1^3}{\nu_{air}^2.T_a} \quad \textbf{(19)}$$

Convective heat transfer coefficient of the heat transfer fluid in the tubes hcf

$$hcf = \frac{Nu.\lambda_{eau}}{D_H} \quad \textbf{(20)}$$

$$Graetz\ number: \quad Gz = Re.Pr.\frac{D_H}{L} \quad \textbf{21)}$$

$$Renolds\ number: \quad R_e = \frac{\rho_{eau} v D_H}{\mu_{eau}} \quad \textbf{22)}$$

$$Prandtl\ number: \quad Pr = \frac{C_p \cdot \mu}{\lambda} \quad \textbf{(23)}$$

- $Laminar\ flow$
- $Gz < 100\ Haussen$

$$Nu = 3.66 + \frac{0.085 \times Gz}{1+0.047 \times Gz^{2/3}} \times \left(\frac{\mu_{eau}}{\mu t}\right)^{0,14} \quad \textbf{(24)}$$

Radiative exchange coefficient between the outer surface of the window and the sky

$$h_{r,ve,ciel} = \sigma \varepsilon_v S_v (T_{ve} + T_{ci})(T_{ve}^2 + T_{ci}^2) \quad \textbf{(25)}$$

The equivalent sky temperature as a function of ambient temperature is given by

$$T_{ci} = 0{,}0552 T_a^{1,5} \quad \textbf{(26)}$$

Radiation exchange coefficient between the glass and the absorber

$$h_{r,v \to ab} = \frac{\sigma (T_{vi} + T_{ab}) \cdot (T_{vi}^2 + T_{ab}^2)}{\frac{1}{\varepsilon_v} + \frac{1}{\varepsilon_{ab}} - 1} \quad \textbf{(27)}$$

Radiation exchange coefficient between the absorber and the tube

$$h_{r,ab \to t} = \frac{\sigma (T_t + T_{ab}) \cdot (T_t^2 + T_{ab}^2)}{\frac{1}{\varepsilon_t} + \frac{1}{\varepsilon_{ab}} - 1} \quad \textbf{(28)}$$

Conduction exchange coefficient at the window

$$h_{cd,v} = \frac{\lambda_v}{e_v} \quad \textbf{(29)}$$

The power absorbed by the glass

$$P_v = \alpha_v I_G S_v \quad \textbf{(31)}$$

The power absorbed by the tube

$$P_{tub} = \alpha_{tub} \tau_v I_G S'_{tub} \quad avec\ S'_{tub} = 3 S_{tub} \quad \textbf{(32)}$$

The power absorbed by the absorber

$$P_{ab} = \alpha_{ab} \tau_v I_G S_{ab} \quad \textbf{(33)}$$

- Thermal efficiency

The instantaneous (or thermal) efficiency of a flat-plate solar collector is equal to the ratio between the useful flux recovered and the total incident irradiance received by the collector surface.(KANOUTÉ et al., 2021)

Output power = Power captured – Losses

$$\eta = \frac{Q_u}{S_{ab} I_G} \quad \textbf{(35)}$$

$$Q_u = \dot{m} c_{pf} (T_{fs} - T_{fe}) \quad \textbf{(36)}$$

4. Results and Discussions

4.1 Experimental results

4.1.1 Experimental temperature profiles of different parts of the solar collector

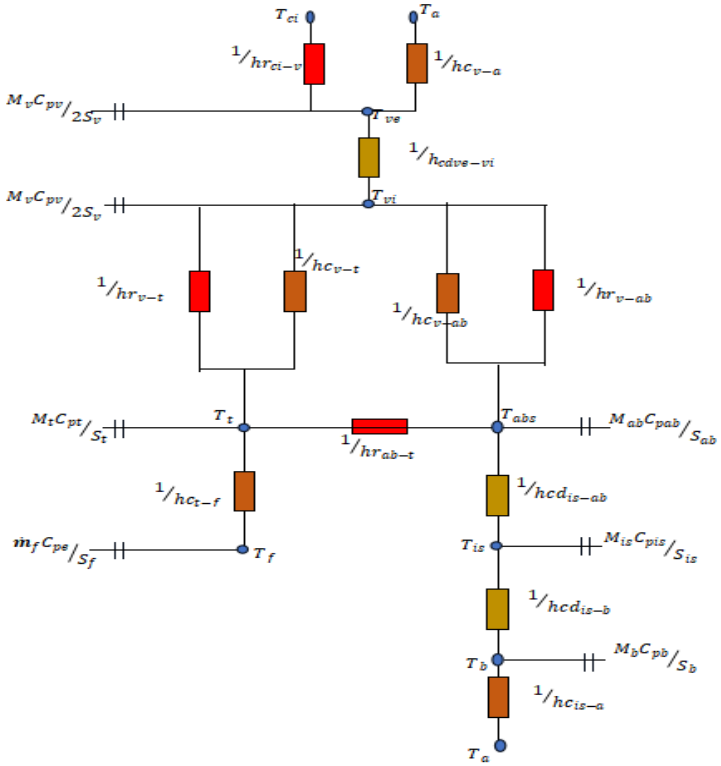

Figure 5 : Temperature changes in different elements

Figure 5 shows that the temperature changes of the various components in the sensor are closely linked to the overall solar radiation received by the sensor. The temperature of the various components rises to reach its maximum between 10:30 a.m. and 4:00 p.m. on the day in question. Overall, we can see that the absorbing plate, which is the main element for capturing radiation, logically has the highest temperature. There is a relatively large temperature difference between the temperature of the fluid at the sensor outlet and that of the absorber plate. This is because the fluid does not exchange heat directly with the plate, but rather with the tubes through which it flows. The curves show that the temperatures of the tubes and the fluid are similar. It can also be seen that the temperature of the insulation is higher than that of the tubes. This may seem paradoxical, as one might implicitly attribute this difference to high losses on the rear side of the absorber, but on the contrary, it is due to

the fact that the tubes transfer heat to the fluid instantaneously. The lowest temperature is that of the outer glass (transparent cover), which is relatively low due to direct contact with the surrounding environment and which gives rise to heat loss by convection with the ambient environment, particularly in the presence of wind. These same observations were made by Bentoumi Hadjer in 2017 in a digital and experimental study of a solar thermal collector in Boussaâda(Bentoumi, 2017).

4.1.2 Changes in average heat transfer fluid temperatures

The curves in Figure 6 below show the evolution of the average temperatures of the heat transfer fluid. These curves have the same shape. From this curve, we can see that on this typical day, the average temperature rises to a maximum of around 40°C. This can be explained by the very low water temperature at the sensor inlet due to the relatively cold climate at this time of year (rainy weather), as noted by Sunday S Nunayon in his study, which found that the performance of solar water heaters is influenced by the climate of the region(Gargab, 2021) and a clear influence of radiation on temperature variation(S.A. Hakem et al., 2008).

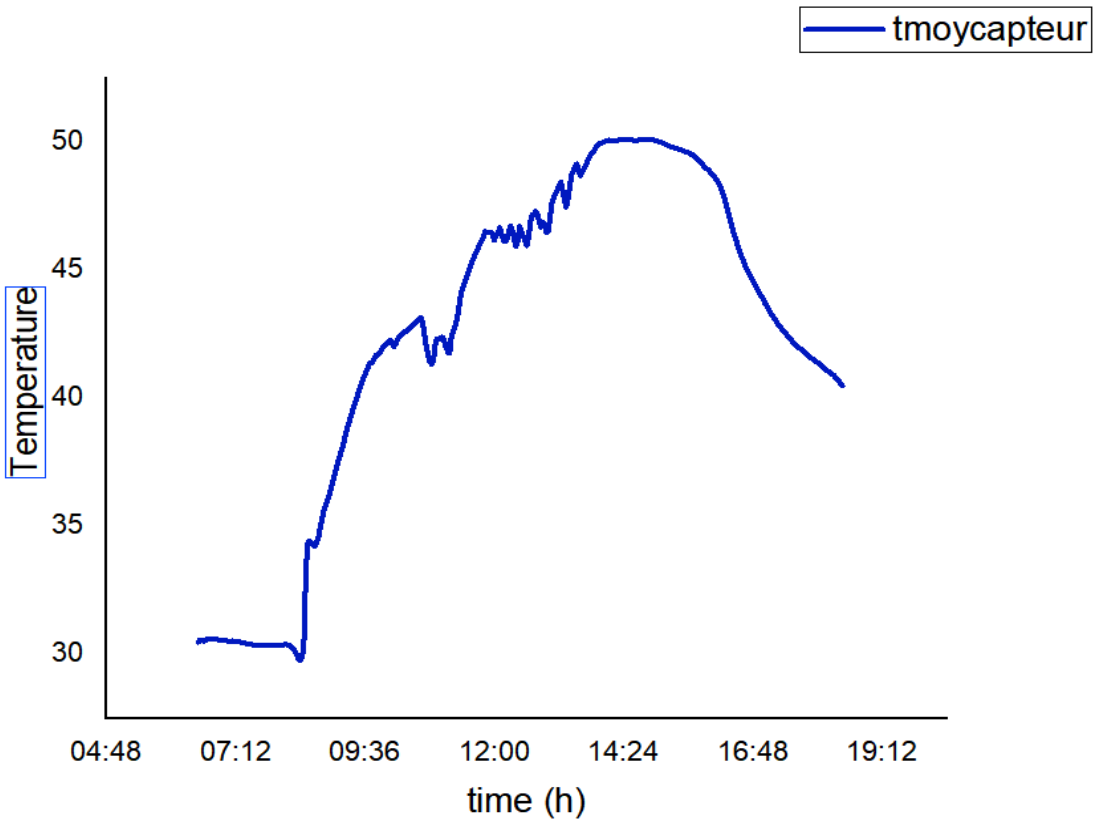

Figue 6 : Temporal evolution of the experimental average temperature of the heat transfer fluid in the collector

4.1.3 Change in instantaneous efficiency over time

Figure 7 shows the curve of the instantaneous yield measured during the day of September 7, 2023. It can be seen that the instantaneous yield increases gradually from sunrise to reach maximum levels between 9 a.m. and 4 p.m., even though sunlight begins to decrease from 1:30 p.m. onwards. Thus, we can see that the performance of the collector does indeed depend mainly on the intensity of sunlight during the day. This trend is also observed by

Sunday S in his study entitled Potential application of a thermosyphon solar water heating system for hot water production in beauty salons: A thermo-economic analysis published in 2022.(Sunday S. Nunayon et al., 2022) At the end of the day, efficiency is around 70%, which is in line with the result obtained by PRIETO et al. of 74%(M.M. Prieto 1 et al., 2016).

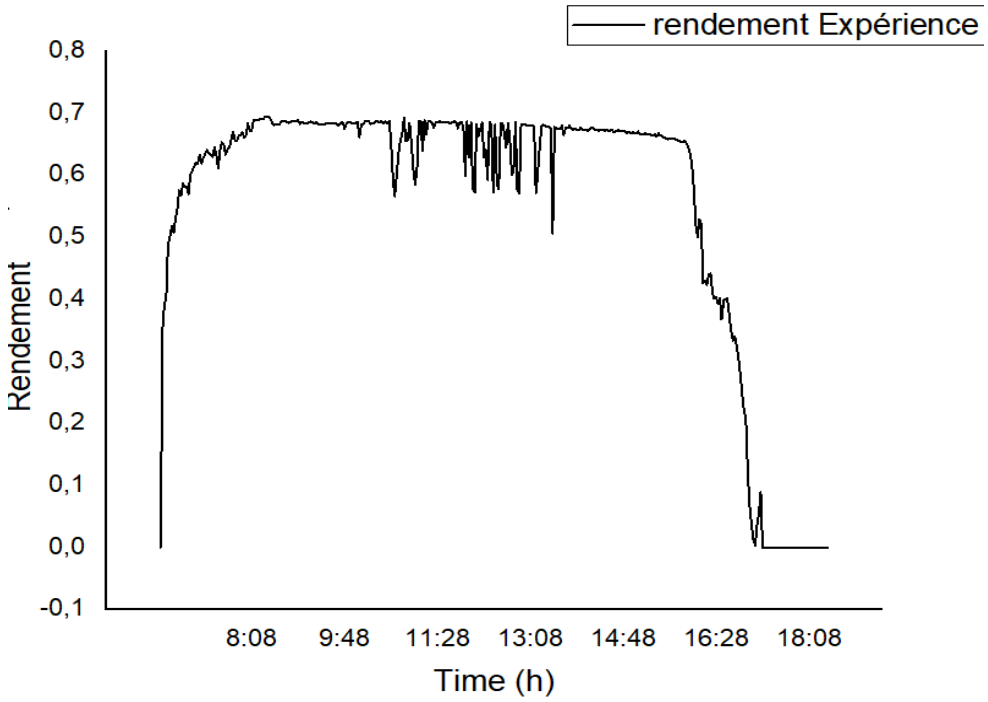

Figure 7 : Hange in instantaneous experimental yield on 09/07/23

4.2 Theoretical results

4.2.1 Temporal evolution of theoretical solar radiation

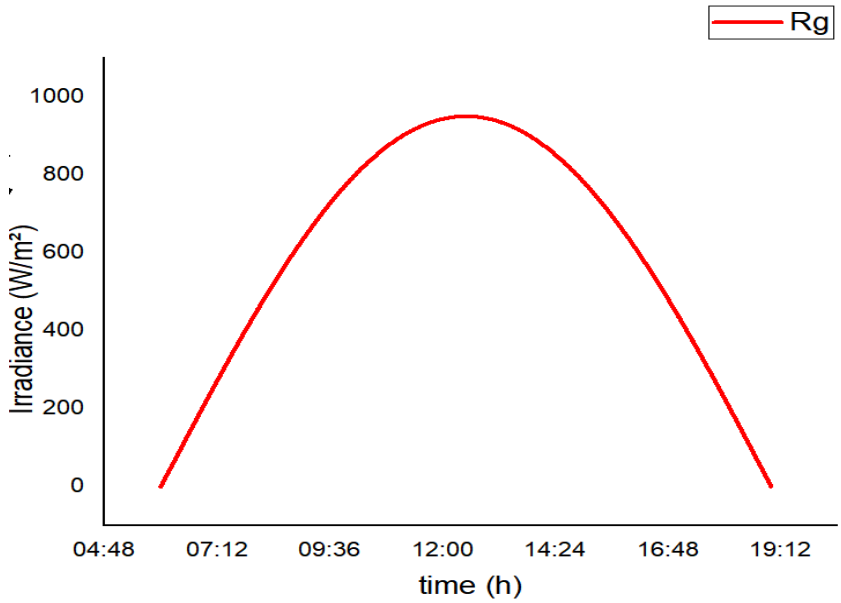

Figure 8 : Temporal evolution of theoretical solar radiation

Figure 8 shows the temporal evolution of global radiation obtained from theoretical data from numerical simulation. It can be seen that the maximum is reached between approximately 12 noon and 2 p.m. This is consistent with the results of several studies conducted on this physical phenomenon(Hamani Nadjette, 2005).

4.2.2 Changes in theoretical temperatures of the various components of the solar collector

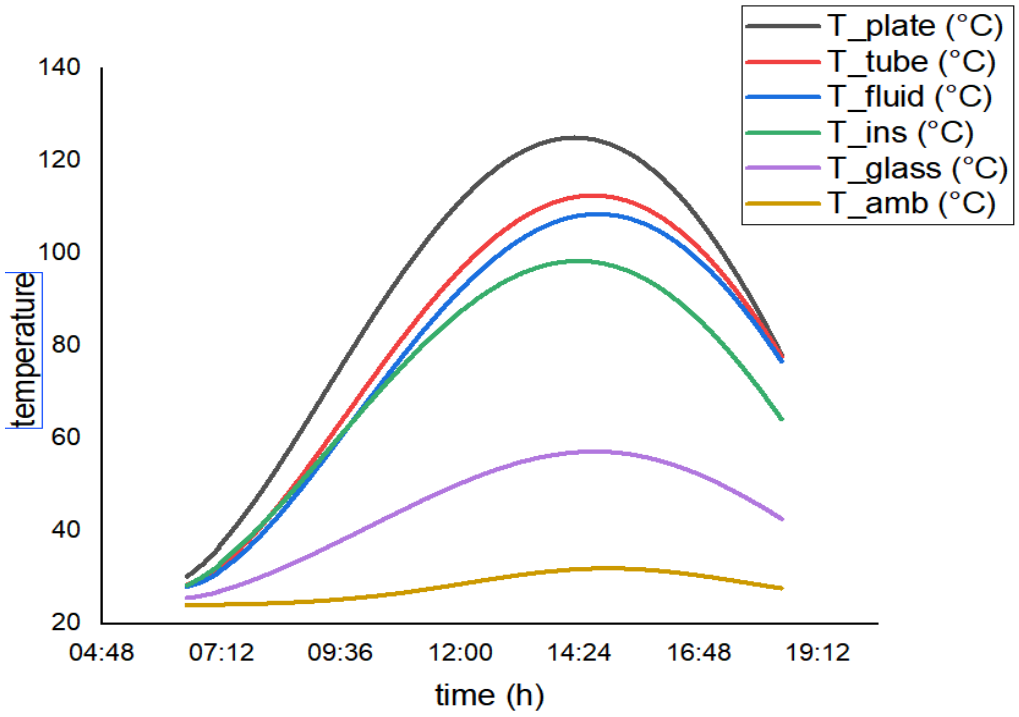

Figure 9 : The evolution of sensor component temperatures based on theoretical data from numerical simulation

The curves in Figure 9 illustrate the temperature evolution of the sensor components based on theoretical data from numerical simulation. These curves show a correlation between the temperature curve of the tubes and that of the heat transfer fluid, which is drinking water. We can therefore conclude that this trend is linked to the fact that the water circulating in the tubes placed on the absorbing plate absorbs its heat to raise its temperature. The numerical results give a fluid close to boiling point. We note that towards the end of the day, the curves for the absorber, the tube, and the fluid merge. This trend is real because these three elements exchange heat directly through the three modes of transfer. This trend in the evolution of the three temperatures was found in the study published by Selvakumar P in 2016(Selvakumar P & Somasundaram P, 2016).

4.2.3 Temperature changes as a function of tube length

The curves in Figure 10 below illustrate the change in temperature of the heat transfer fluid (water) in the tubes that act as heat exchangers in the solar collector at different positions along the tube. It can be seen that the temperature increases with the length of the tube. For example, for a length of 0.50 m, a maximum temperature of 40°C is reached, compared to 50°C for a length of 2 m, a considerable difference of 10°C. Thus, the performance of the solar collector is optimized according to the length of the tubes and, indirectly, the number of tubes.

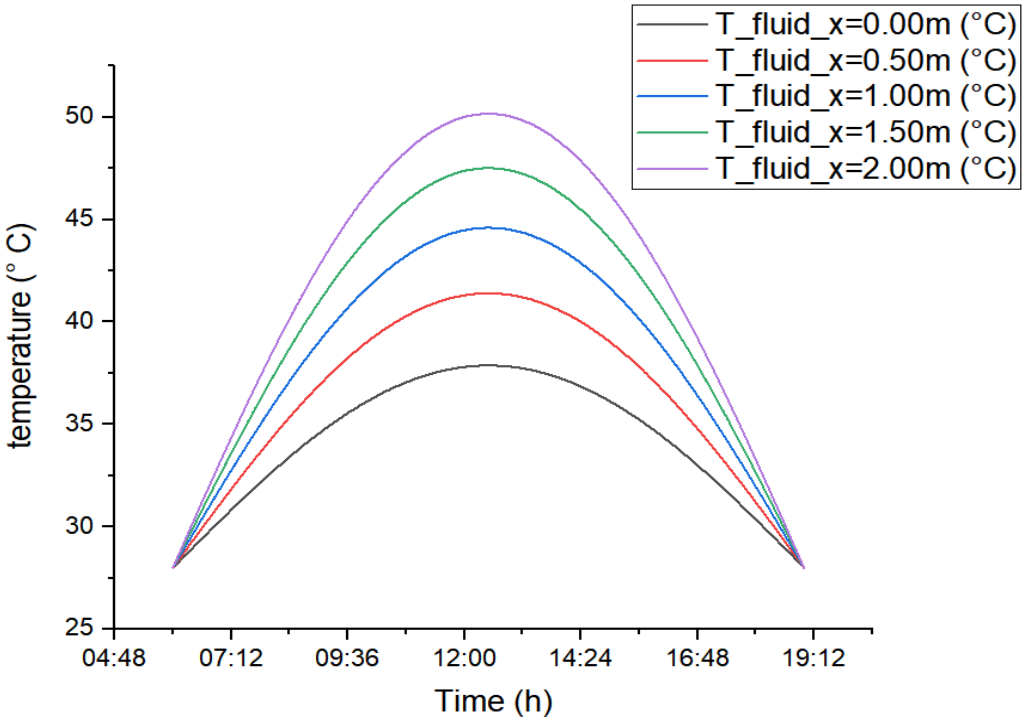

Figure 10 : Temperature changes as a function of tube length

4.2.4 Change in theoretical average temperature and instantaneous numerical efficiency

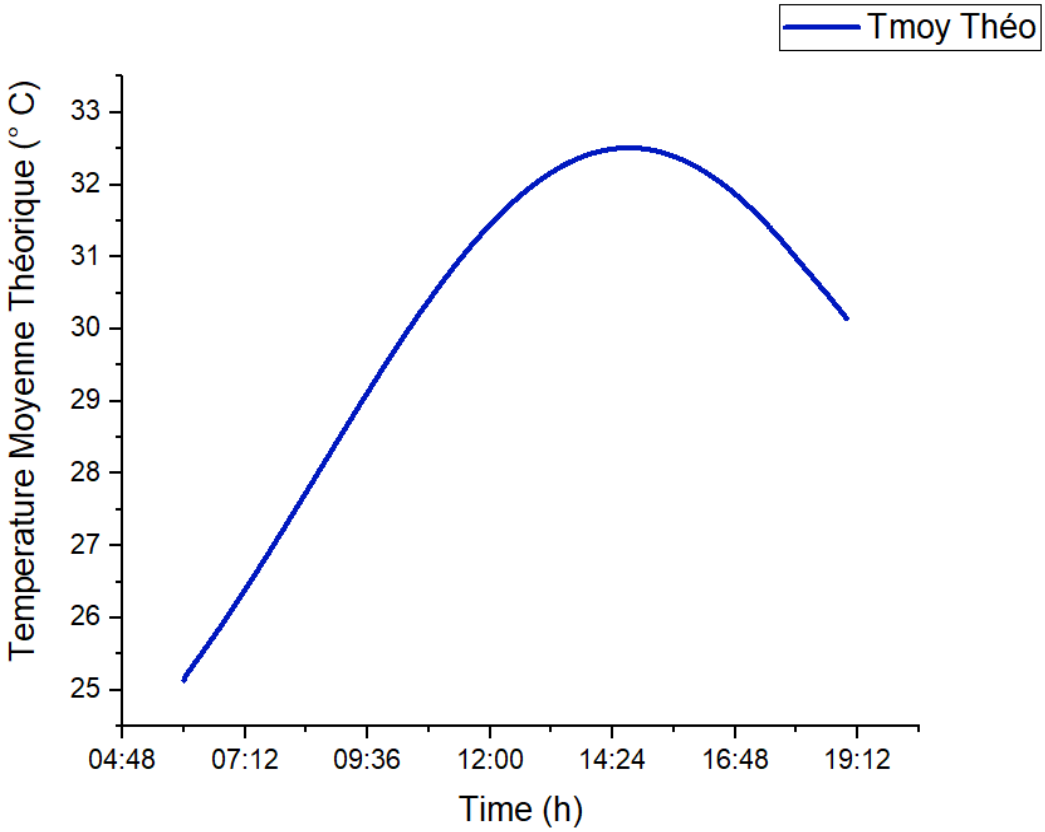

Figure 11 : Change in theoretical average temperature

Figures 11 and 12 show the evolution of the theoretical average temperature and the theoretical yield, respectively, based on data from the numerical simulation of the solar collector. In Figure 11, the curve indicates a maximum average temperature of around 33°C. This lower maximum is due to the thermal characteristics of galvanized steel, which is less thermally efficient than other materials such as aluminum and copper. Furthermore, in the model, the inlet water temperature is fixed, whereas in reality the system operates in a closed loop. Consequently, the inlet temperature varies throughout the day as it depends on the temperature of the tank

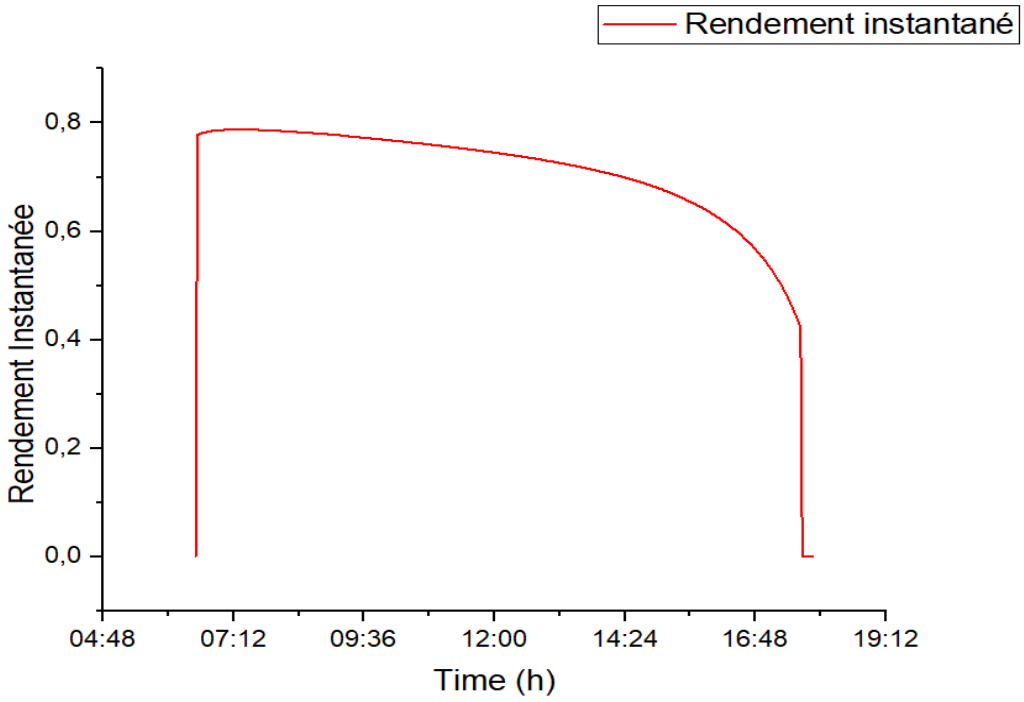

Figure 12 : The theoretical instantaneous yield of the collector during the day

Figure 12 shows the theoretical instantaneous efficiency of the sensor throughout the day. The curve shows three major phases. An upward phase in the morning due to the onset of sunlight. Thus, the sensor's performance increases when the inlet temperature is low.(Sunday S. Nunayon et al., 2022) A horizontal phase during most of the day shows constant sensor performance when there is sunlight, and a downward phase at sunset shows that the thermosiphon effect, which depends on the temperature gradient, has stopped. This curve trend was obtained by Sunday S. The theoretical results give a maximum efficiency of 78%.

4.2.5 Mass flow rate variation over time

It can be seen that the variation in flow rate closely follows the profile of solar radiation, reaching a maximum of 0.06 kg/s. Three phases can be observed in the curve (Figure 13): an ascending phase and a descending phase corresponding respectively to the periods of increasing and decreasing sunlight on the sensor during the day. The three roughly horizontal phases correspond to the period of the day when the fluid temperature gradient is almost stationary due to the strong solar radiation accumulated on the absorber. These results are similar to those of the model developed by H. Abdi and N. Aït Messaoudène (H. Abdi & N. Aït Messaoudène, 2000).

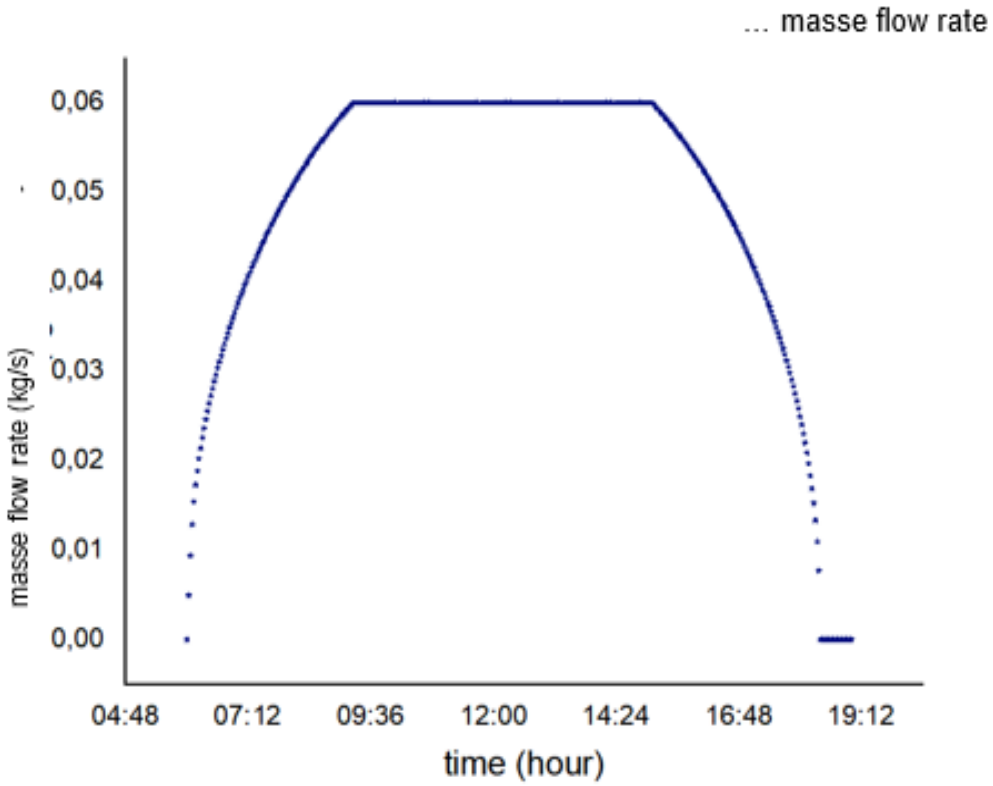

Figure 13 : Mass flow rate evolution over time

4.2.6 Change in instantaneous efficiency as a function of mass flow rate

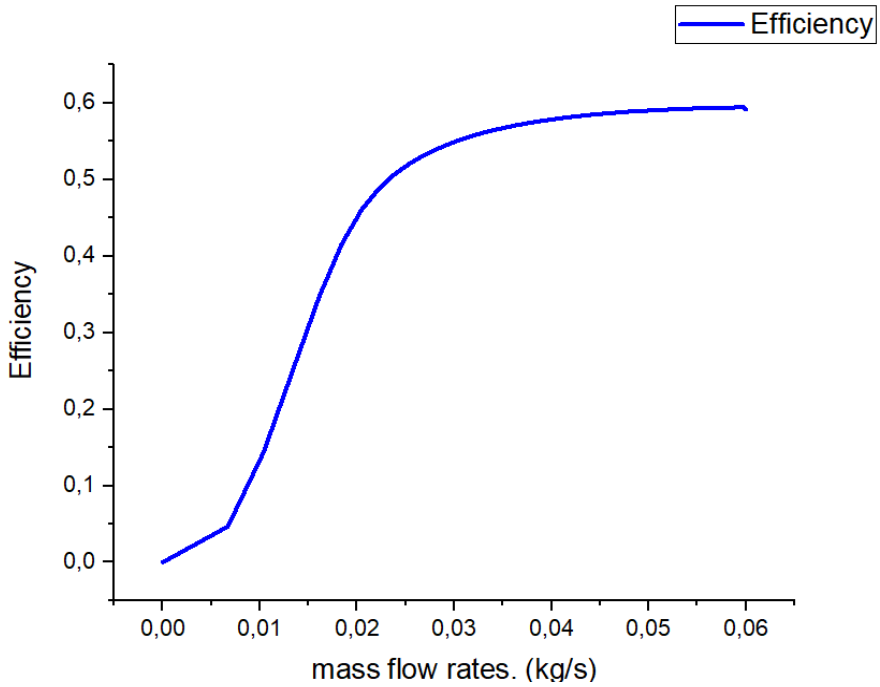

Figure 14 : Change in instantaneous efficiency as a function of mass flow rate

Figure 14 shows the sensor's performance profile as a function of mass flow rate. Two phases can be observed, indicating rapid growth in performance when the flow rate is below 0.015 kg/s and a quasi-stationary phase for higher flow rates. This leads to the conclusion that this type of flat-plate sensor is well suited to thermosiphon operation, which corresponds to low flow rates, in order to improve performance. The result is identical to that found by Thiago P. Lima et al.(Thiago P. Lima et al., 2015).

4.2.7 Fluid temperature variation as a function of mass flow rate

Figure 15 illustrates the changes in the water outlet temperature (A) and heat loss (B) curves for the solar collector. Curve (A) shows a decreasing outlet temperature profile and an increasing loss (B) profile as the mass flow rate increases. This is justified because the higher the heat loss, the less heat the water receives.

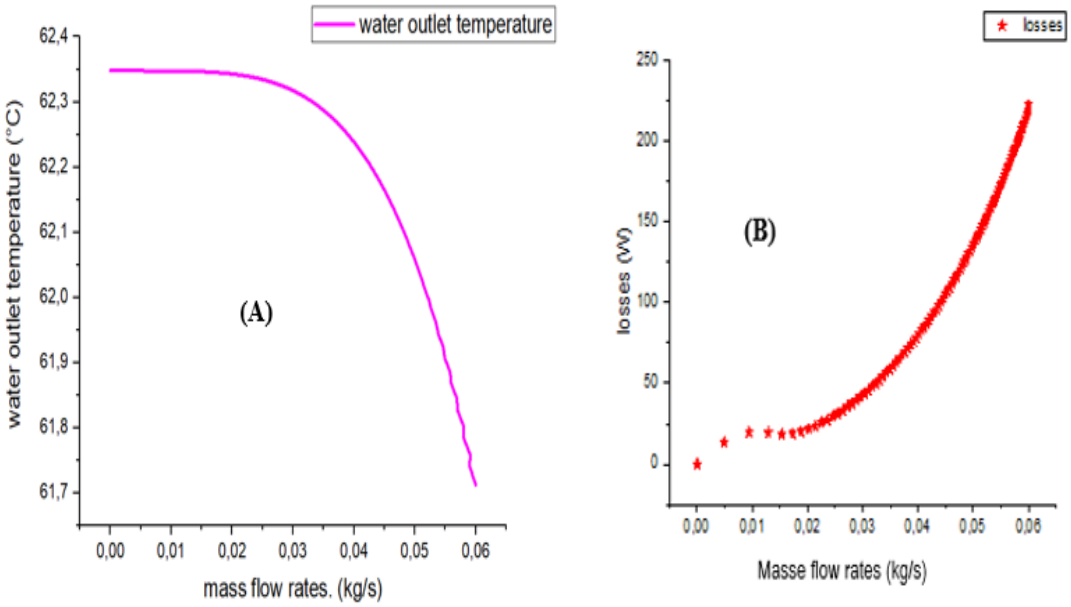

Figure 15 : Change in outlet water temperature (A) and losses (B)

4.3 Validation of numerical and experimental results

Figure 16 shows the profile of the temporal evolution of digital and experimental global radiation. Overall, the trend shows realistic conformity. Indeed, we note that sunshine reaches its maximum between 11 a.m. and 2 p.m. on both curves, which is consistent with many results in the literature (Abdellatif Oudrane, 2018) and S.A. Hakem et al.

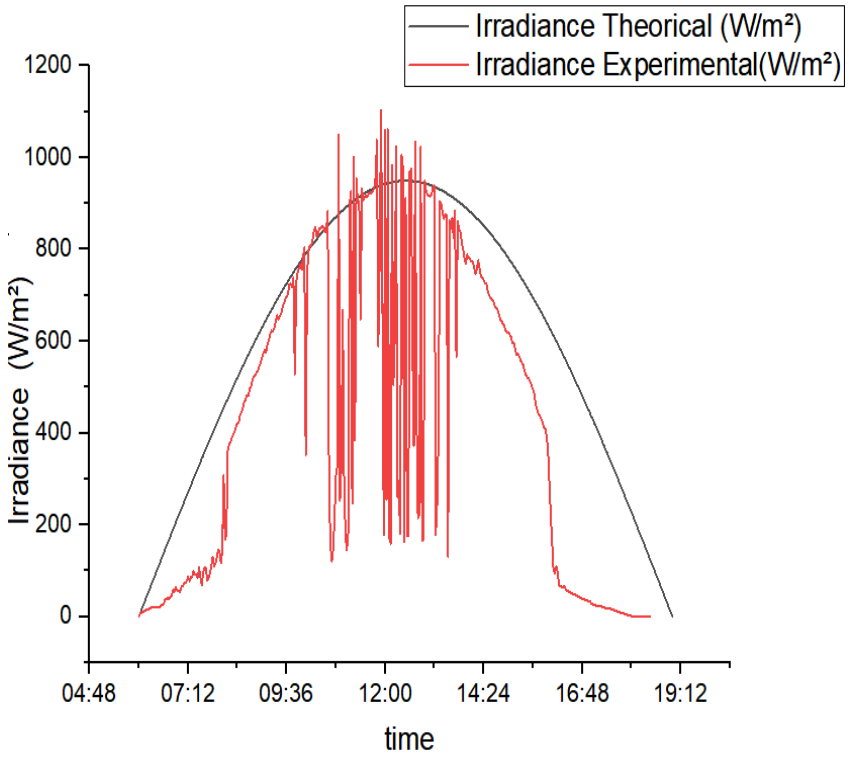

Figure16 : Profile of the temporal evolution of numerical and experimental irradiance.

Figure 17 illustrates the variation over time of the experimental and theoretical temperatures of the solar collector components. These curves show similarities for each component and are consistent with those already established by Selvakumar et al.(Selvakumar P & Somasundaram P, 2016). There is therefore a good correlation between the experimental and theoretical temperatures, with a correlation coefficient of approximately 0.97.

Figure 17 : Changes in theoretical and experimental temperatures of solar collector components solaire

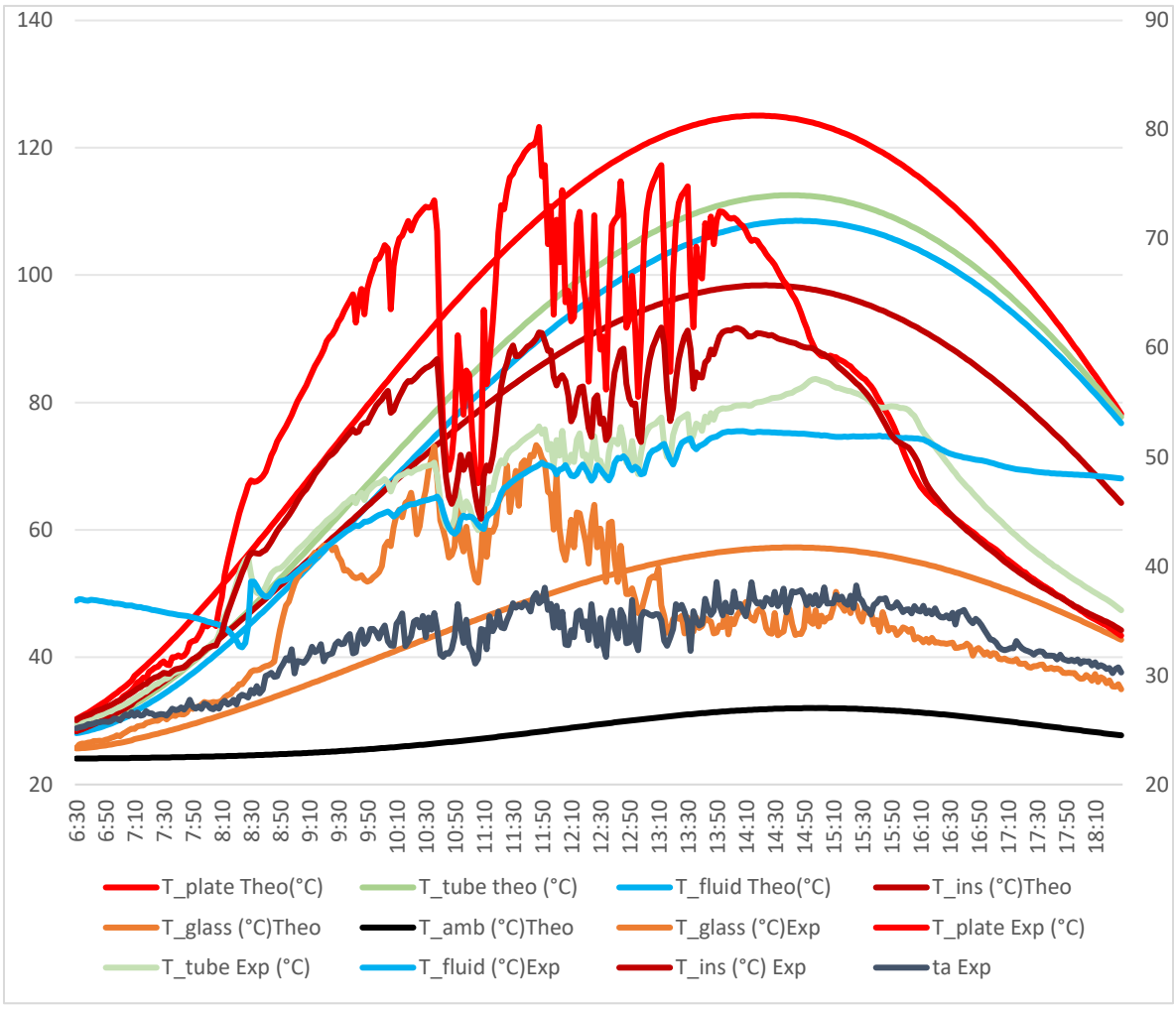

Figure 17 : Changes in theoretical and experimental temperatures of solar collector components solaire

Similarly, Figures 18 show a trend in the evolution of the theoretical and experimental average temperature curves with a correlation coefficient of around 0.92 and a relative average error (RAE) of 14%.

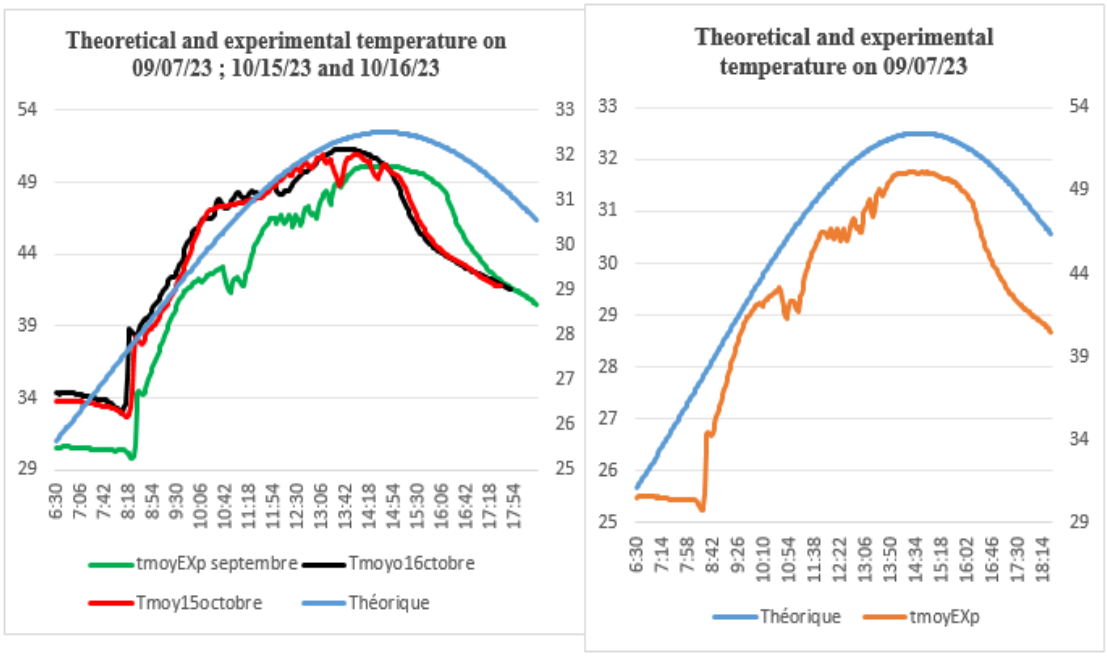

Figure18. : Evolution of the theoretical and experimental average temperature curves

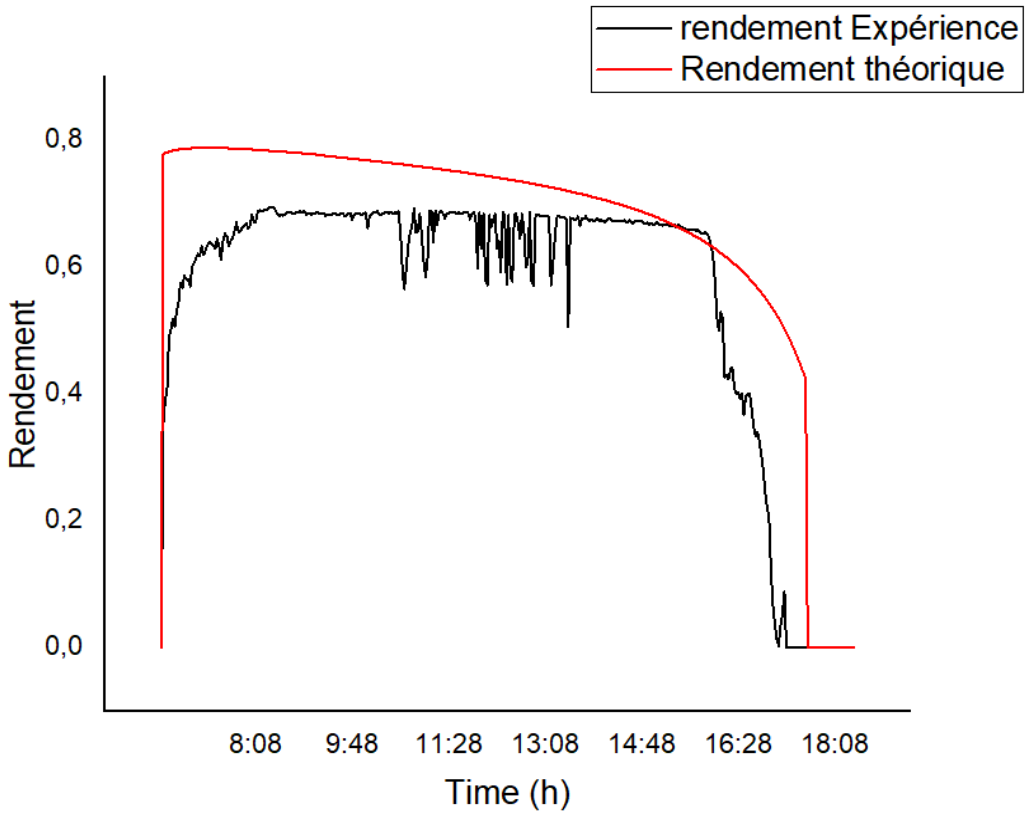

Figure 19 : Theoretical and empirical instantaneous yield curves

As for the yield curves, Figure 19 illustrates a trend between the theoretical and experimental yields. Both curves clearly show the three phases during the day and reach a maximum of 80% and 70% for the theoretical and experimental yields, respectively. The results obtained are compared with those of another conventional system available on the market, which consists of a flat plate collector and a storage tank placed vertically or horizontally, and are consistent with those found by Ahmed Aisa (Ahmed Aisa & Tariq Iqbal, 2016).

It can be seen that the curve in **Figure 20** is a straight line, which is consistent with the literature by Safaa Mohammed Ali Mohammed Reda et al. in 2024(Safaa Mohammed Ali Mohammed Reda et al., 2024). This shows that the forward heat loss coefficient does not vary significantly. The maximum efficiency obtained is 0.70 for experimental performance and 0.9 for theoretical performance. This can be explained by the fact that the smaller the difference between the average temperature of the tank and the average ambient temperature, the greater the efficiency(B. Chaouachi* & et S. Gabsi, 2006).

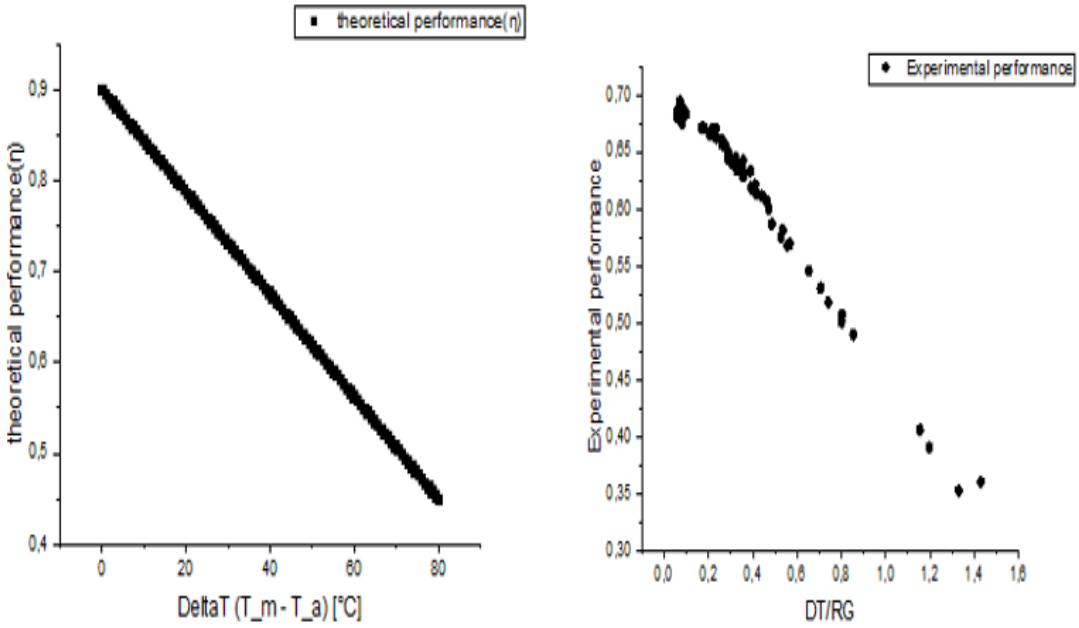

Figure 20 : Variation in the theoretical and experimental efficiency of the system over the course of a day

Figure 21 shows the theoretical and experimental power curves for the solar collector. This figure clearly shows that the curves have similar profiles, with a maximum of approximately 800 W for the experimental power compared to 1400 W for the theoretical power. This difference reflects the impact of the climatic conditions recorded on the solar collector during the tests during this rainy period in Burkina Faso. It also shows that the collector can provide more useful power to raise the water temperature under better conditions. There is also a similarity between the solar radiation curve and the useful power delivered by the solar collector. These results are consistent with those of Koffi in 2013(koffi, 2013) and VASSILIS BELESSIOTIS(VASSILIS BELESSIOTIS & EMMANOUIL MATHIOULAKIS, 2002), which demonstrates that the performance of the collector depends greatly on external thermal parameters such as solar irradiance, ambient temperature, and wind speed. ambient temperature, and wind speed....

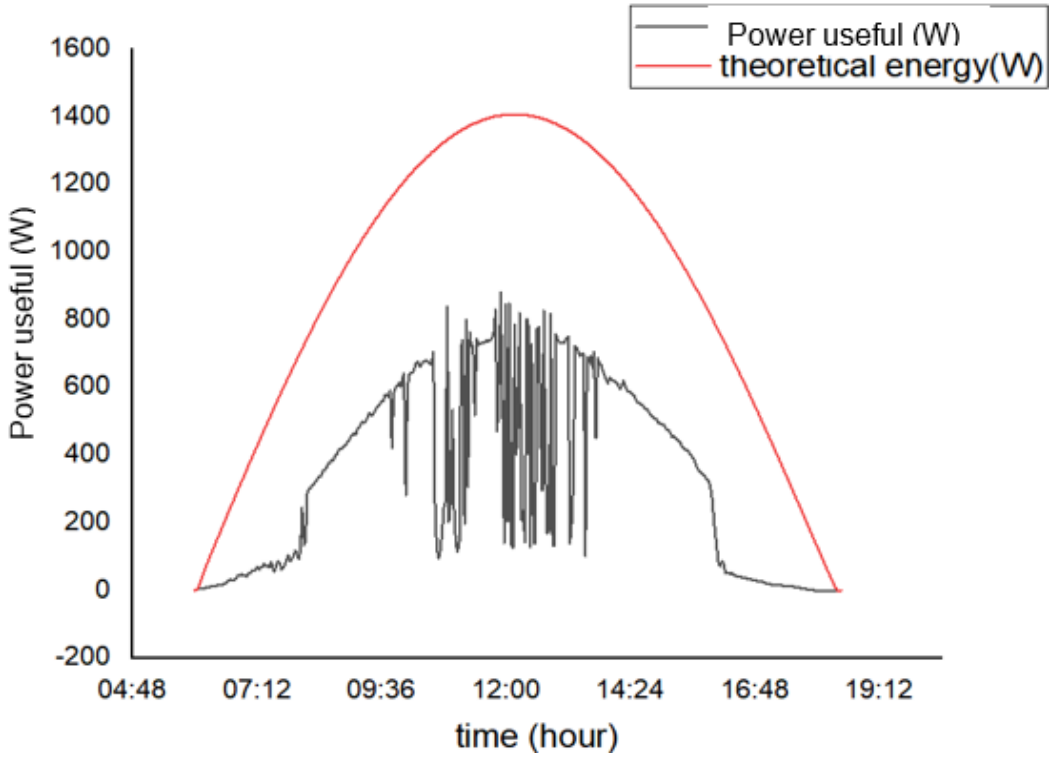

Figure 21 : shows the theoretical and experimental power curves for the solar collector

5. Conclusion

This study enabled us to develop a digital model, simulate a number of external and internal parameters affecting the efficiency and temperature of the flat-plate solar collector, and compare these results with the results of measurements taken during the rainy season under the meteorological conditions of Burkina Faso. Thanks to the experimental study, we were able to evaluate the instantaneous efficiency, useful power, and temperature behavior of the flat-plate solar collector components (absorber plate, heat exchanger tube, glazing, insulation, and fluid), as well as the overall solar radiation. The operation of the various components of our solar water heater is linked to global solar radiation. The results showed that the maximum instantaneous efficiency is 70% with a maximum global solar radiation of 1101W/m2 and a maximum ambient temperature of 39.64°C. The temperatures of the collector components range from 40°C to 72°C. Finally, the temperature of the heat transfer fluid at the outlet varies between 39°C and 60°C. The numerical results showed that the temperature increases with the length of the tube; the influence of radiation on the efficiency and useful power of the collector and, consequently, on the mass flow rate of the fluid.

Nomenclature

hc:convection coefficient and the tube

hct-f: between the tube and the heat transfer fluid.

hcb-a: between the external insulation and the ambient air.

*e*1= distance between the glass and the absorber [m]

λair= thermal conductivity of air [W.m^{-1}.K^{-1}]

Nu= the average Nusselt number

Gr : Grashoff dimensionless number

$vair$= The kinematic viscosity of the confined air [m2.s^{-1}]

g = acceleration due to gravity [m.s^{-2}]

= The difference between the respective temperatures of the upper surface of the absorber and the inner surface of the glass [K].

Ta= Ambient temperature [K]

Re: Reynolds number

Pr: Prandtl number

eis= thickness of the insulation [m]

λis= thermal conductivity of the insulation [W.m^{-2}.K^{-1}]

= thickness of the glass [m]

= thermal conductivity of the glass [W.m^{-1}.K^{-1}]

$Ptub$: Power absorbed by the tube

Pab: Power absorbed by the absorber

$Stub$: Surface area of the tubes

Qu: Useful flux recovered by the heat transfer fluid (W).

Cpf: Specific heat of the heat transfer fluid (J/kg K).

IG: Solar irradiance (W/m^2)

Mab: The mass of the absorber

Is:$Irradiation\ solaire$ (W/m^2

β:$facteurs\ optique$ (%)

κ: $coefficient\ de\ transmissio\ n\ thermique$ ($W\ /m^2.K$)

Tm:$Température\ moyenne\ du\ ca\ pteur\ K$

Ta :$température\ ambiante\ K$

Te: $Température\ entrée\ capteurK$

Ts: $température\ sortie\ capteur\ k$

α:$taux\ d'absorptionde\ l'\ absorbeur$%

τ: $Taux\ de\ transmission\ du\ vit\ rage$ (%)

Tve: $Température\ de\ la\ vitre\ exte\ rne°C$

Tvi: $Température\ de\ la\ vitre\ inte\ rne°C$

$Ttub$:$Température\ du\ tube°C$

$Tabs$: $Température\ de\ la\ plaque\ abs\ orbante\ °C$

Tec:$Température\ de\ l'\ eau\ entrant\ dans\ le\ capteur°\ C$

Tsc:$Température\ de\ l'\ eau\ sortant\ dans\ le\ capteur°\ C$

Tf:$la\ température\ de\ l'\ cau\ froide°C$

V: $le\ volume\ \ représente\ les\ bes\ oins\ en\ L/j$

C: $la\ puissance\ \ qui\ représente\ les\ besoins\ en\ kWh/j$

Tc:$la\ température\ de\ l'\ cau\ chaude°C$

Tis:$Température\ de\ l'isolant\ °C$

References

Abdellatif Oudrane. (2018, March 5). *Contribution à la Modélisation et au Développement des Systèmes de Chauffage Solaire à Usage Individuel*. Ecole Nationale Polytechnique d'Oran - Maurice Audi République Algérienne. Thèse pour l'Obtention du Titre de Doctorat Es-Science en Génie Mécanique

Ahmed Aisa, & Tariq Iqbal. (2016, October). *Modelling and Simulation of a Solar Water Heating System with Thermal Storage*. DOI:10.1109/IEMCON.2016.7746283

Armand Noël Ngueche Chedop, Noël Djongyang, & Zaatri Abdelouahab. (2018). *Modelisation Et Etude Comparative Des Capteurs Solaires Plans Et A Tubes Dans Les Regions Soudano-Saheliennes Du Cameroun.* https://www.researchgate.net/publication/324878121

ARSE - Burkina Faso. (n.d.). Retrieved 19 November 2024, from https://www.arse.bf/

Article_KABORE_Elixir (2).pdf. (n.d.).

B. Chaouachi*, & et S. Gabsi. (2006, June 21). Etude expérimentale d'un chauffe-eau solaire à stockage intégré dans des conditions réelles. *Revue des Energies Renouvelables Vol. 9 N°2 (2006) 75 - 82*.

Bentoumi, H. (2017, 05). *Etude numérique et expérimentale d'un capteur solaire thermique en Boussaâda*. UNIVERSITE MOHAMED BOUDIAF - M'SILA REPUBLIQUE ALGERIENNE D.

BOUALAMALLAH, Hd., Merdji, A., ,GHAZI, A., & Miloudi, A. (2021). Optimisation d'un chauffe- eau solaire. *Revue Des Matériaux et Energies Renouvelable*, *Vol 6, N°1, 2022*. Journal home : https://www.univ-relizane.dz

Gargab, F. Z. (2021). *Technical-economic optimization and manufacture of a Moroccan solar water heater.* [Phdthesis, Université de Pau et des Pays de l'Adour ; Université Sidi Mohamed ben Abdellah (Fès, Maroc). Faculté des sciences]. https://theses.hal.science/tel-03278007

H. Abdi, & N. Aït Messaoudène. (2000). Etude Expérimentale et Théorique des Performances de deux Capteurs Plans à Contact Direct Eau-Plaque d'Absorption. *Rev. Energ. Ren. : Chemss 2000 53-60*. Institut de Mécanique, Université de Blida, B.P. 270, Route de Soumaa, Blida

Hamani Nadjette. (2005). *Modélisation du flux solaire incident et de la température de sortie dans un capteur solaire à eau avec effet de concentration du rayonnement solaire incident.* Université Mohamed Khider-Biskra,REPUBLIQUE ALGERIENNEEn Vue de l'Obtention du Diplôme de Magister En Physique du Solide.

John A. Duffie (Deceased) & William A. Beckman. (2013). *Solar Engineering of Thermal Processes*.

KANOUTÉ, Y., Traore, I., Sanogo, S., Aroudam, E., & BA, A. (2021). Optimisation du rendement et de la température d'un capteur solaire plan à eau par simulation. *Journal de Physique de La SOAPHYS*, *2*, C20A03-1. https://doi.org/10.46411/jpsoaphys.2020.01.03

koffi, P. M. E. (2013, February 24). Thermal performance of a solar water heater with internal exchanger using thermosiphon system in Côte d'Ivoire. *journal homepage: www.elsevier.com/locate/energy*. . http://dx.doi.org/10.1016/j.energy.2013.09.059

KY, J.-B. (2024). *ARSE - Burkina Faso*. https://www.arse.bf/

M. Bouragbi Lakhdarn. (2024, March 27). *Conception Et Optimisation Des Performances D'un Capteur Solaire Plan*. Badji-Mokhtar-Annaba University Universite Badji-Mokhtar-Annaba. t: https://www.researchgate.net/publication/379333251

Michel Daguenet. (1985). *les séchoires solaires: Théorie et pratique*.

M.M. Prieto 1, B. González 2, & E. Granado 2. (2016, June 15). *Thermal performance of a heating system working with a PCM plate heat exchanger and comparison with a water tank*. https://doi.org/10.1016/j.enbuild.2016.03.078

S.A. Hakem, N. Kasbadji–Merzouk, & M. Merzouk. (2008). Performances journalières d'un chauffe eau solaire. *Revue des Energies Renouvelables CICME'08 Souss*. hakem.sidali@cder.dz

Safaa Mohammed Ali Mohammed Reda, Dheya Ghanim Mutasher, & Wajeeh K. Hasan. (2024). Enhancing Thermal Efficiency in Solar Water Heaters: The Role of Reflective Walls. *Mathematical Modelling of Engineering Problems Vol. 11, No. 4, April, 2024, Pp. 893-902 Journal Homepage: Http://Iieta.Org/Journals/Mmep*. https://doi.org/10.18280/mmep.110406

Selvakumar P, & Somasundaram P. (2016). Experimental Analysis on Solar Water Heater with Corrugated Absorber for Enhanced Heat Transfer. *Journal of Thermal Energy Systems Volume 1 Issue 2*. E-mail: kecselvakumarp@gmail.com

Sunday S. Nunayon, *, & , Williams P. Akanmu. (2022). Potential application of a thermosyphon solar water heating system for hot water production in beauty salons: A thermo-economic analysis. *Case Studies in Thermal Engineering*. https://doi.org/10.1016/j.csite.2022.101881

Thiago P. Lima, Jose Carlos C. Dutra, & Ana Rosa M. Primo. (2015). Solar water heating for a hospital laundry: A case study. *ScienceDirect Solar Energy 122 (2015) 737–748*. http://dx.doi.org/10.1016/j.solener.2015.10.006

Vassilis Belessiotis, & Emmanouil Mathioulakis. (2002). *Analytical Approach of Thermosyphon Solar Domestic Hot Water System Performance*.

Tables

Table 1 : Components of a solar water heater

matériaux	**Density (kg m^{-3})**	**thickness (mm)**	**Thermal capacity (J kg-1 K-1)**
water	1000	-	4180
glass	2530	5	840
Collector plaque	7800	1.5	470
Collector Tuber	7800	2	470
Isolant interne	40	30	840
Air	1.2	40	1006

Table 2 : Physical properties of solar collector components materials

Collector	Galvanized steel
Glazing	ransmissibility: τ_V= 83%
Clear glass	Reflexibility: 8 %
	Absorptivity: α_V=9%
Tilt angle	15°
	Length: L=2 m
Collector dimensions	*Width: l=1 m*
	Gross surface area:
	S=2 m²
	Length: L_t=1.80 m
Pipe dimensions	*Diameter D_H:15 mm*
	Diameter: d_t=21 mm
	Number: 12
Maximum operating temperature	T_{max}=95 °C

Table 3 : Thermal properties of solar collector components

	glass	Collector plaque	Collector tuber	Laine de verre	Heat transfer fluid	air
Viscosity dynamics (Pa·s)		-	-	-	$1{,}00 \cdot 10^{-3}$	$1{,}81 \cdot 10^{-5}$
absorptivity	**0.02**	**0.95**	**0.95**		-	-
conductivity ($W\,m^{-1}\,K^{-1}$)	**0.78**	50	46.7	0.041	**0.6**	**0.023**
Emisivity	**0.89**	0.16	0.04	0.85	-	-